This is an Accepted Manuscript of an article published by Taylor & Francis in Attia, N., Santos, E., Abdelmouty, H., Arafa, S.A., Zohdy, N., Hernández, R.M., Orive, G., & Pedraz, J.L. (2014). Behaviour and ultrastructure of human bone marrow-derived mesenchymal stem cells immobilised in alginate-poly-l-lysine-alginate microcapsules. Journal of Microencapsulation, 31, 579 - 589.https://doi.org/10.3109/02652048.2014.898706

Behavior and ultrastructure of human bone marrow-derived mesenchymal stem cells immobilized in alginate-poly-L-lysine-alginate microcapsules

Noha Attia[1*], Edorta Santos[2,3*], Hala Abdelmouty[1], Samia Arafa[1], Nahed Zohdy[1], Rosa María Hernández[2,3], Gorka Orive[2,3], José Luis Pedraz[2,3]

[1]Department of Histology and Cell Biology, Faculty of medicine, Alexandria University, Alexandria, Egypt; [2]NanoBioCel Group, Laboratory of Pharmaceutics, University of the Basque Country, School of Pharmacy, Vitoria, Spain; [3]Biomedical Research Networking Center in Bioengineering, Biomaterials and Nanomedicine (CIBER-BBN), Vitoria, Spain.

*****These two authors contributed equally to the study.

Correspondence should be addressed to: José Luis Pedraz (joseluis.pedraz@ehu.es)

Laboratory of Pharmacy and Pharmaceutical Technology
Faculty of Pharmacy UPV/EHU
Paseo de la Universidad nº 7
01006 Vitoria-Gasteiz, Spain
Phone: +34-945013091
Fax: +34-945013040

Running title: Ultrastructure of encapsulated mesenchymal stem cells.

Abstract

Context: Human bone marrow mesenchymal stem cells (hBM-MSCs) show a great promise for the treatment of a variety of diseases. Despite the previous trials to encapsulate hBM-MSCs in alginate-poly-L-lysine-alginate (APA) systems, the various changes that follow immobilization have not been ascertained yet.

Objective: Determine the various consequences derived from entrapment on cell behavior, putting special emphasis on the ultrastructure.

Methods: hBM-MSCs were immobilized in APA microcapsules to further characterize their viability, metabolic activity, proliferation, VEGF-secretability, and morphology.

Results: The VEGF produced by monolayer hBM-MSCs increased significantly one day post-encapsulation, and was maintained for at least four weeks. TEM imaging of cells revealed well preserved ultrastrucure indicating protein synthesis and high metabolic activity.

Conclusion: Although APA microencapsulation did not support 100% of fully viable hBM-MSCs for long-term cultures, it was conceived to enhance both VEGF secretion and metabolic activity while not losing their stemness characteristics.

Key words: Bone marrow-derived mesenchymal stem cells, Alginate, Cell microencapsulation, VEGF secretion, Ultrastructure.

INTRODUCTION

Human bone marrow mesenchymal stem cells (hBM-MSCs) are considered promising adult multipotent stem cell populations (Giordano et al., 2007). They are able to differentiate both into multiple mesoderm- and non-mesoderm-type lineages (Sanchez-Ramos, 2002; Baksh et al., 2004). Unlike other bone marrow (BM) resident cells, they can be easily isolated by their selective adherence to culture vessels. MSCs represent an ideal candidate for cell-based therapies as they are a robust cell type exhibiting a remarkable genetic stability (Karaöz et al., 2011). Moreover, they can interact with cells of both the innate and adaptive immune systems, leading to the modulation of several effector functions (Griffin et al., 2010). MSCs are well known for their hypoimmunogenic properties (Nauta and Fibbe, 2007). They were found to immunoregulate cytotoxic T lymphocytes, both directly and indirectly (Beyth et al., 2005). Furthermore, they can significantly affect the progression of autoimmune diseases, as they are involved in alloantigen recognition and elimination (Abumaree et al., 2012). Finally, as adult stem cells, clinical applications of MSC bring up a powerful alternative to ethically controversial use of embryonic stem cells (Chan et al., 2007).

In addition to their intrinsic “stem” properties for cell-based therapy, numerous lines of evidence suggest that MSCs secrete several soluble factors, which can stimulate the regeneration of surrounding microenvironment after local transplantation (Phinney and Prockop, 2007; Horie et al., 2011). Among these factors, vascular endothelial growth factor (VEGF) is a key pro-angiogenic factor that increases vascularization and perfusion, thus considered one of the key players behind clinical improvement of

patients with myocardial infarction, limb ischaemia, or stroke that receive MSC therapy (Nagaya et al., 2004). MSCs are well known for their capacity to home to injured tissues, differentiate into distinctive cell types, and promote the formation of regenerative microenvironments (Jones and McGonagle, 2008). However, even if systemic delivery of MSCs appears to be a safe, clinically relevant approach for cell therapy, Pittenger and Martin have shown that less than 3% of MSCs delivered by direct injection were still present after two weeks (Pittenger and Martin, 2004). Such a low cell survival, together with the poor organ-specific cell retention and the difficulty to control the phenotype of transplanted cells over sufficiently long times, have greatly hampered the success of cell-based therapies (Menasché, 2005; Correa et al., 2007).

For over a decade, researchers have explored the use of alginate hydrogels as artificial extracellular matrices to encapsulate living cells and improve their transplantation (Orive et al., 2005; Ponce et al., 2006). These scaffolds provide a more natural 3D microenvironment for the cells, resembling in vivo situation where cells develop their function (Abbah et al., 2008). Alginate is considered one of the biomaterials of choice for many researchers (Garate et al., 2012), since their hydrogels are non-cytotoxic, semi-permeable, and have been shown to provide immune protection for many cell types (Yu et al., 2010). Furthermore, alginate allows gel formation under gentle conditions, which is an attractive feature for cell encapsulation (Orive et al., 2006). Entrapped cells can be thoroughly studied, as they consistently achieve a longer lifespan in culture compared with non-encapsulated cells (Ghidoni et al., 2008). Transplantation of encapsulated MSCs -as a measure to immunoisolate them- can

open the door for the use of non autologous cells, allogenic or even xenogenic (Ngoc et al., 2011).

In this work, we aimed to encapsulate hBM-MSCs into APA microcapsules in order to further characterize cell behavior in terms of viability, metabolic activity, proliferation and VEGF secretion. In addition, we also investigated the impact of microencapsulation on their morphology, ultrastructure, and preservation of their differentiation potential following recovery at different time intervals.

METHODS

Monolayer culture of hBM-MSCs

P1 cryopreserved hBM-MSCs (24 years old female donor) were obtained from the Texas A&M Health Science Center College of Medicine Institute for Regenerative Medicine at Scott & White through a grant from NCRR of the NIH, grant # P40RR017447. Primary hBM-MSCs were cultured at 500-1000 cells/cm^2 in T-175cm^2 tissue culture flasks (Corning) maintained at 37°C in a humidified 5% CO_2 environment. Cells were cultured in Complete Culture Medium (CCM) composed of Alpha Minimum Essential Medium (α-MEM; Invitrogen) supplemented with 16.5% fetal bovine serum (FBS, Gibco), 1% L-glutamine (Gibco), and 1% Antibiotic-Antimycotic (Gibco). All experiments were conducted on cells at passage 2 – 4 with medium changed twice a week.

Encapsulation

hBM-MSCs were immobilized into APA microcapsules using an electrostatic droplet generator (8 V) with brief modifications of the procedure designed by Lim and Sun (Lim and Sun, 1980). Ultra pure low-viscosity and high-guluronic acid alginate (LVG) was purchased from FMC Biopolymer, Norway, and poly-L-lysine (PLL; hydrobromide MW= 15-30 kDa) was obtained from Sigma-Aldrich (St. Louis, MO, USA). Briefly, cells were harvested from monolayer cultures using trypsin- EDTA 0.25% (Gibco), filtered through a 40 μm pore mesh and resuspended in 1.5% (w/v) LVG-alginate sterile solution, obtaining a cell density of $5x10^6$ cells/mL. This suspension was extruded through a 0.35 mm needle using a 10 mL sterile syringe with a peristaltic pump (flow rate 5.9 mm/h). The resulting alginate beads were collected in a $CaCl_2$ solution (55 mM) and maintained in agitation for 10 min for complete ionic gelation. Subsequently, the beads were coated with 0.05% (w/v) PLL for 5 min, followed by a second coating with 0.1% alginate for another 5 min. Finally, the microcapsules were cultured in CCM. The whole process was carried out at room temperature (RT) and under aseptic conditions. The diameters and overall morphology were characterized using inverted optical microscopy (Nikon TSM).

Characterization of hBM-MSCs before and after encapsulation

1. In vitro adipogenic and osteogenic differentiation

As for pre encapsulated hBM-MSCs were seeded onto 6-well plates (BD Falcon) for 2 weeks with medium changed twice a week till 70-80% confluence. After 2, 4, and 6

weeks of encapsulation, cells were de-encapsulated with 0.5 mg/mL of alginate lyase (Sigma-Aldrich) and cultured in CCM till 70-80% confluence. The same differentiation protocol was applied on all samples. For Adipogenic differentiation, hBM-MSCs were cultured in CCM supplemented with 0.5 μM Dexamethasone (Sigma-Aldrich), 0.5 μM isobutylmethylxanthine (Sigma-Aldrich), and 50 μM Indomethacin (Sigma-Aldrich). For osteogenic differentiation, cells were cultured in CCM supplemented with 10 nM Dexamethasone, 20 mM β-glycerolphosphate (Sigma-Aldrich) and 50 μM L-ascorbic acid 2-phosphate (Sigma-Aldrich). After two weeks differentiation protocol, intracellular lipid droplets indicating adipogenic differentiation were confirmed by Oil Red O (ORO) (Sigma-Aldrich) staining. Osteogenic differentiation was assessed by staining with Alizarin Red S (ARS) (Sigma-Aldrich).

2. CFU assay

One hundred pre-encapsulated hBM-MSCs were cultured in 10 ml of sterile CCM in a 100 mm diameter dish (about 55 cm^2 culture area). Cells were incubated for 14 days, with medium change twice a week. Then, the plate was stained with 3 % Crystal Violet in 100% methanol to distinguish colonies. The same assay was repeated on de-encapsulated hBM-MSCs after 6 weeks of entrapment.

Encapsulated cell viability and proliferation

1. Live /Dead assay

Encapsulated cells were stained with the LIVE/DEAD kit (Invitrogen) and after incubation for 30 min in dark at RT, fluorescence micrographs were taken with an epi-fluorescence microscope (Nikon TSM). Live cells fluoresced in green via enzymatic conversion of acetoxymethyl ester of calcein (calcein-AM) to calcein, while the nuclei of dead cells fluoresced in red via labeled Ethidium homodimer-1 (EthD-1) due to the impairment of the cell membrane integrity. This assay was performed on days 1, 14, and 42 post-encapsulation.

2. Flow cytometry for quantitative assessment of cell viability

hBM-MSCs were de-encapsulated with 0.5 mg/mL of alginate lyase and filtered through a 40 µm mesh filter. Free cell suspension was added to TrueCount® tubes (BD) and stained with 1 µM calcein-AM and 0.8 mM EthD-1 (LIVE/DEAD kit). After 20 min incubation in dark at RT, cell viability was assessed by means of flow cytometry (BD FACSCalibur). The population corresponding to de-encapsulated cells was gated in a FSC/SSC dot plot and further analyzed in a bivariate FL1/FL3 dot plot. The signal of green fluorescing calcein was detected in the FL1 channel, while FL3 channel was employed for red fluorescing EthD-1. Calcein positive and EthD-1 negative cells (upper left quadrant) were considered viable, calcein negative and EthD-1 positive cells (lower right quadrant) were considered dead. However, both

calcein and EthD-1 positive (upper right quadrant) were considered as living damaged cells. TrueCount® beads were utilized for calculation of cell concentration per sample. This assay was performed on days 1, 14, and 42. CellQuest Pro software was used both for acquisition and analysis of the data. For all samples, a total of 1 x10^4 events were examined. Data were shown as mean of 3 independent samples ± S.D.

3. Cell Counting Kit-8 (CCK-8) assay

Metabolic activity was determined on the basis of tetrazolium production using the Cell Counting Kit-8 (CCK-8) (Sigma-Aldrich). For all samples, this assay was performed on days 1, 7, 14, 21, 28, 35, and 42. For 2D hBM-MSCs, cell suspensions were seeded at 3000 cells per well in 12-well plates and incubated in 5%CO_2, 37 °C. At predetermined time points, wells were washed twice with phosphate-buffer saline (PBS). 500 µL of CCM were added to each well with 50 µL of CCK-8. After 4h incubation, color development was read at 450 nm using a Tecan M200 microplate reader. All values were corrected with the reference wavelength at 690 nm and normalized against the mean value of 3 blank wells (only CCM). Samples were examined in triplicates. Data were shown as mean of 3 independent samples ± S.D. As for the microcapsules, same procedure was carried out by inoculating 100 µL of microcapsule suspension per well in a 96-well plate, and followed by addition of 10 µL of CCK-8. Samples were examined in triplicates. Data were shown as mean of 7 independent samples ± S.D.

4. Cell Proliferation Assay

Cell proliferation was monitored by 5-Bromo-2'-deoxyuridine (BrdU) incorporation during DNA synthesis by using a BrdU-based cell proliferation ELISA. Briefly, The equivalent of 2×10^4 cells/100 µL medium were placed into each well of 96-well plate, incubated with CCM supplemented with 10% FBS. The negative control groups were incubated with starving medium (supplemented with 0.1% FBS). After 24 h, the microcapsules were incubated in the presence of 10 µM BrdU for an additional 24 h. Cells were de-encapsulated with 0.5 mg/mL of alginate lyase and assayed for BrdU uptake using Cell Proliferation Biotrak ELISA System (Amersham, NJ, USA) following manufacturer's instructions. Absorbance was quantified at 450 nm using a Tecan M200 microplate reader. Absorbances of the non-specific binding control groups (without BrdU) were subtracted from the rest of the groups, and results were normalized with the corresponding negative control for each experiment. Data were shown as mean of 5 independent samples ± S.D per study group.

VEGF secretion

50 µL of microcapsules/mL were inoculated into each well in a 6-well plate, and subsequently incubated for 48 h. The same procedure was repeated for 2D hBM-MSCs by placing 15 000 cells/mL in each well. The VEGF concentration in the culture supernatants of both 2D and encapsulated cells was determined using a Quantikine Human VEGF Immunoassay ELISA Kit (R&D Systems, Minneapolis, MN, USA) according to the manufacturer's instructions. All assays were performed in triplicate, and the results were expressed as mean ± SD.

Phalloidin staining for F actin

Phalloidin was used to detect F-actin in encapsulated cells 2 and 4 weeks post-encapsulation. Microcapsules were washed with PBS and fixed for 10 min with 3.7% paraformaldehyde (Sigma-Aldrich). After washing twice with PBS, cell membranes were permeabilized with 0.1% Triton X-100 (Sigma-Aldrich) for 5 min and then washed again with PBS. Samples were then incubated in a 6.6 mM Alexa Fluor®488 phalloidin (Molecular Probes) and 1% BSA solution for 40 min at RT and protected from light in order to label F-actin component of the cytoskeleton. Finally, samples were washed with 1% BSA in PBS solution. Microcapsules were observed under confocal laser scanning microscope (CLSM; LEICA LCS SP2 AOBS).

Transmission Electron microscopy (TEM)

Monolayer cell pellets and microcapsules were fixed with 2% gluteraldehyde in PBS (pH 7.4) for 24 h at 4°C, washed and post-fixed with 1% OsO_4 buffered with 0.1 mol/L PBS for 2 h. All samples were dehydrated in a graded series of ethanol and embedded in Epon 812. Ultrathin sections (90 nm) were double-stained with uranyl acetate and lead citrate and then examined with PHILIPS EM208S TEM.

Statistical analysis

In BrdU uptake test, Mann Whitney test was used to compare samples with control groups, and Wilcoxon Signed Ranks Test was used to compare results of day 10 with those of day 30. Additionally, Mann Whitney test was also used to compare VEGF

secretion between (monolayer- day1 microcapsules), and (monolayer- day 28 microcapsules), while Wilcoxon Signed Ranks Test was used to compare between day1 microcapsules and day 28 microcapsules. A (∗) indicated significant difference between groups for statistical significance of $P \leq 0.05$.

Results

Characterization of pre-encapsulated hBM-MSCs

The pre-encapsulated hBM-MSCs were morphologically characterized. Results showed a heterogeneous population of cells exhibiting large, flattened, or fibroblast-like shapes as shown in Fig. 1(A). After 3–4 days of incubation, cells gradually proliferated into small colonies [Fig. 1(B)], which increased after two weeks of culture to form larger and interconnected colonies [Fig. 1(C)].

Adipogenic differentiation potential of hBM-MSCs was confirmed by positive intracellular lipid droplets stained with ORO, while osteogenic differentiation was documented by the presence of amorphous material deposits positively stained with ARS, which indicated calcium content [Fig. 1(D), (E)].

Microcapsule morphology and encapsulated cell viability

Elaborated microcapsules had uniform and spherical morphology (diameter: 600–650 μm). On days 1, 14, and 42 post-immobilization, cell viability was assessed microscopically after LIVE-DEAD kit staining. Green dots represented living cells,

while red dots represented the nuclei of dead cells. As shown in Fig. 2, the majority of cells appeared viable and evenly dispersed throughout the microcapsule with no clustering. For more accurate assessment of cell viability and determination of viable cell number per capsule, flow cytometric analysis was applied on the encapsulated cells at the same time-points. Flow cytometric analysis estimated an average number of (199±13) living cells per capsule one day post-encapsulation 83.3 %± 5.6, which decreased to (133±23) 55.5 %± 9.6 after 2 weeks. At the end of the experiment, the number of living cells per capsule was (29±3) 11.9 %± 1.2. Upper right quadrants depicted cells positive for both calcein and Ethd-1, suggesting their plasma membrane alteration. Interestingly, the percentage of these cells was also decreasing.

Cell behavior and functionality

Since it is known that the extracellular matrix influences the behavior of encapsulated cells, we aimed to study the consequences of encapsulation on some cell functions. The metabolic activity of both cells in monolayer and cells within the microcapsule was analyzed in vitro over the course of 6 weeks. hBM-MSCs plated onto flat substrates showed a gradual increase in reading until the fourth week reaching a plateau thereafter [Fig. 3(A)], whereas encapsulated hBM-MSCs revealed an initial decrease in their metabolic activity after one week of encapsulation followed by a stable metabolic activity until the end of the experiment [Fig. 3(B)].

Immobilized cells were assayed for DNA synthesis in order to detect evidence of cell proliferation. As denoted in Fig. 3(C), encapsulated cells demonstrated no significant BrdU

incorporation when compared against negative controls, neither on day 10 nor on day 30 post-encapsulation ($P>0.05$).

Among various cytokines produced by hBM-MSCs, VEGF was considered of particular interest as a potent angiogenic factor, holding the potential for treating various disorders. In the current study, quantitative assessment of VEGF production via encapsulated hBM-MSCs was done to probe any possible variation in cell functionality upon entrapment. Fig. 3(D) reflected the release profile of VEGF from both monolayer and immobilized hBM-MSCs. The secretion was normalized to 10^6 cell/ mL/ 48h to allow direct comparisons between groups. Monolayer cells produced 9.53±1.54µg/mL of VEGF, while the same number of immobilized cells one day post-encapsulation secreted up to 23.23±1.39µg/mL ($P=0.05$). Four weeks later, the secretability of encapsulated hBM-MSCs (20.74±5.86 µg/mL) did not exhibit significant changes ($P>0.05$).

Morphological and Ultrastructural characterization

In this study we aimed to detect any morphological alterations of hBM-MSCs immobilized in non-modified alginate matrix. Enclosed hBM-MSCs' morphology was assessed using CLSM after staining cellular F- actin with Alexa Fluor 488-Phalloidin. As illustrated in Fig. 4, cells depicted short cytoplasmic projections after two weeks of immobilization, becoming more prominent by the fourth week.

TEM was applied to detect any variations in the ultrastructure of immobilized cells. Electron micrographs of monolayer hBM-MSCs showed eccentric, irregularly shaped

and large euchromatic nuclei with prominent nucleoli. The chromatin was dispersed except for a thin dense layer located immediately inside the perinuclear membrane. The cytoplasm was rich in rough endoplasmic reticulum profiles (rER) with dilated cisternae containing moderately electron dense material. The cell surface showed several thin pseudopodia. The presence of many clear vacuoles gave the periphery of the cytoplasm a multilocular appearance [Fig. 5(A), (B)]. After two weeks of encapsulation, the general ultrastructure of cells was not changed except for the appearance of alginate filaments internalized within the vacuoles [Fig. 5(C), (D)]. The same finding was also seen after four weeks of encapsulation, in addition to the appearance of lysosomes, giant and normal-sized mitochondria [Fig. 5(E)] together with marginated nucleolus [Fig. 5(F)].

Differentiation potential of de-encapsulated hBM-MSCs

The ability of encapsulated cells to retain their stem cells properties upon de-encapsulation was evaluated. These cells retained both adipogenic and osteogenic differentiation potential as confirmed by ORO and ARS staining respectively [Fig. 6(A)]. Additionally, hBM-MSCs de-encapsulated after 6 weeks of encapsulation were observed to retain their pre-encapsulation morphology and colony forming ability [Fig. 6(B)].

Discussion

hBM-MSCs are truly attractive adult cells, which reside in specialized but still largely unknown tissue compartments "niches" (Shin and Peterson, 2012). They have been in focus of many researchers in the field of medicine for decades due to their enormous therapeutic potential and stable properties. Since MSCs cultured in vitro onto 2D substrates (e.g. "tissue culture plastic") may lose cell-specific properties with time and so, poorly reflect their behavior in vivo (Han et al., 2012), in this study we aimed to elucidate various facets of hBM-MSC behavior within one of the most studied 3D scaffolds, "alginate microcapsules". Few studies have attempted to encapsulate hBM-MSCs, even though their homing capacity, hypoimmunogenic and immunomodulatory properties make them likely the cells of choice in therapeutic cell encapsulation. Moreover, none have focused on the ultrastructural alterations that may occur to those cells upon encapsulation. In the current work, hBM-MSCs were encapsulated into APA microcapsules, and then were thoroughly characterized as regards their viability, metabolic activity, proliferation, VEGF secretability, and morphology, putting special emphasis on cellular ultrastructure.

In any microencapsulation-based cell therapy strategy, the accurate assessment of the viability and proliferation of encapsulated cells is essential for predicting the potential long-term secretion profiles of their therapeutic products. In the present study, Live/Dead kit was used to assess cell viability both by microscopy and by flow cytometry. Even though the microscopic evaluation depicted no clear difference in green fluorescing dots between day 1 and 14, flow cytometry - as a much accurate assay- demonstrated reduction of cell viability over time. Grossmann (Grossmann,

2002) explained such decreasing viability of immobilized cells by the lack of appropriate cell-matrix adhesion, thereby increasing detachment-induced cell death (anoikis). Similar to epithelial and endothelial cells, MSCs are anchorage-dependent cells in which cell-extracellular matrix interaction plays a paramount role in their survival and function (Rowlands et al., 2008).

Metabolic activity of monolayer cells increased gradually, reaching a plateau after 4 weeks. Such pattern was expected in light of the consensus that once the MSCs reach confluence, their rate of proliferation decreases (Neuhuber et al., 2008). On the other side, immobilized cells showed an initial decrease in the metabolic activity/capsule after one week of encapsulation, followed by a plateau. Thus, given the gradual decline in cell viability together with the absent cell proliferation, present results denoted a gradual increase of cellular metabolic activity after 2 weeks of entrapment till the end of the experiment. The fore mentioned cessation of mitotic activity in encapsulated cells was in accordance with other researchers reporting that encapsulated MSCs had minimal space for growth and, thus, became contact-inhibited and growth arrested (Markusen et al., 2006; Duggal et al., 2008). In turn, Bidarra et al. (Bidarra et al., 2010) had attributed such lack of cell proliferation to the spatially constraining polymeric network. Moreover, Ma and co-researchers (Ma et al., 2003) documented that MSCs seized to proliferate upon immobilization. Additionally, they reported that alginate encapsulation provides a suspension condition, unsuitable for division of the anchorage-dependent MSCs, thus became arrested in G0G1 phase. G1-arrested cells are metabolically more active than non-arrested ones (Hu and Zeng, 2012) and such increased cellular metabolic activity could refer to cell activities other than proliferation (Bidarra et al., 2010). On the other hand, our data were not in

agreement with those of Goren and co-workers (Goren et al., 2010). Those authors reported that the viability and proliferation of the encapsulated hBM-MSCs remained stable throughout their 70 days-experiments. Discrepant findings could be explained by the different experimental design (for example, lower alginate concentration and/or much lower cell density) compared to that adopted in the current study.

Beneficial effects of hBM-MSCs are believed to be mainly due to their paracrine activity, so that we next investigated if APA-encapsulated hBM-MSCs would retain their pre-encapsulation paracrine function. Several research groups documented the ability of monolayer MSCs to secrete VEGF and other angiogenic cytokines (Tang et al., 2006; Burchfield and Dimmeler, 2008; Boomsma and Geenen, 2012). Moreover, Bidarra and colleagues (Bidarra et al., 2010) proved that the VEGF secreted by encapsulated MSCs was able to diffuse through the hydrogel network into the surrounding medium. However, to the best of our knowledge, this is the first study performing direct quantitative comparison between VEGF secretability of pre- and post-encapsulated hBM-MSCs. We discerned what it seems to be a significant upregulation of VEGF secretion after encapsulation that was retained even after 4 weeks of culture. Lee and co-workers (Lee et al., 2013) have recently explained such increased VEGF secretion by the relative hypoxic environment inside the microcapsules. Additionally, several micro-environmental cues such as shear stress and substrate compliance have been reported to control MSC paracrine activity (Ranganath et al., 2012). Anyway, the molecular forces that increase the secretory function of encapsulated hBM-MSCs are intriguing but still unclear.

Contrary to expectations, our results showed that hBM-MSCs embedded in non-modified alginate matrix attained several µm-sized cortical protrusions into the surrounding matrix that became more evident by the fourth week of encapsulation. Those filopodia-like branches were further evidenced by fluorescent staining of actin filament. Since the alginate hydrogel used for encapsulation was not modified with adhesion moieties, such cellular extensions could not be due to cell-matrix adhesion, as reported by other several studies (Lawson et al., 2004; Markusen et al., 2006; Bidarra et al., 2010; Sayyar et al., 2012). On the other side, the ultrastructural findings revealed by the current study, reflected the presence of endocytotic vesicles within the encapsulated cell cytoplasm with alginate filaments internalized. In previous studies (Tso et al., 2010; Gorbunov et al., 2012), it has been shown that BM-MSCs depict actin-dependent phagocytic capacity, which could explain the endocytosed alginate, the prominent lysosomes "as terminal compartments of the endocytic pathway", and eventually the filipodia discerned with confocal microscopy. The pore size of gelled, high guluronic acid content alginate is almost large than 200 nm. This is sufficient to allow monovalent cations such as sodium and potassium in cell culture media to diffuse into the matrix, thereby destabilizing the ionic interactions that hold the hydrogel together (Hunt et al., 2010). The individual destabilized strands of alginate - seen in TEM results- were small enough for MSCs to begin sequestering them. Despite such limited degradation, the hydrogels could retain sufficient mechanical integrity to exhibit gel-like properties that allows sustained immobilization of cells (Nunamaker et al., 2007). Further ultrastructural characteristics of hBM-MSCs revealed their developed and metabolically active nature similar to those published by other research groups (Pasquinelli et al., 2007; Karaöz et al., 2011). Moreover, the observation of giant mitochondria in four weeks-encapsulated cells may justify such

increased metabolic activity. Some publications reported the presence of normal-sized and huge mitochondria in metabolically active and secretory cells with normal architecture (Spicer et al., 1990; Tandler et al., 1997). Dilated rER cisternae, discerned both before and after encapsulation, denoted active synthesis of proteins all through the experiment; attesting that the encapsulation per se did not hinder the cellular protein synthesis. In light of the results of Grayson et al. (Grayson et al., 2006), hypoxic microenvironment could have induced increased total protein levels in encapsulated MB-MSCs. Additionally, marginated nucleoli seen 4 weeks post-encapsulation could support the enhanced secretory nature of cells. Margination of nucleoli was reported in cells with an active ribosomal RNA production (Sasaki et al., 1983; Wachtler et al., 1986; Montironi et al., 1991). In their review, Kumar and colleagues (Kumar et al., 2007) reported that cellular protein production is dependent on the phase of the cell cycle and various genes such as those involved in ribosome biogenesis are expressed highly in the G1 phase. Therefore, the G1-phase of the cell cycle is considered the ideal time for increased production of proteins (Hu and Zeng, 2012). In essence, ultrastructural findings could support the improved metabolic activity and functionality of immobilized cells on both secretory and phagocytic domains.

In the current study, it was evident that the encapsulation process neither abolished the colony forming capacity of de-encapsulated cells, nor their mesodermal differentiation potential, which was in agreement with previous studies (Goren et al., 2010; Baraniak and McDevitt, 2012). The choice of the mesodermal differentiation assay was based on the fact that The Mesenchymal and Tissue Stem Cell Committee of the International Society for Cellular Therapy considered the multipotent

differentiation potential as the property that most uniquely identifies MSC (Dominici et al., 2006). On the other hand, CFU assay was done to ensure that the encapsulation-induced proliferation arrest was halted after recovery. Being able to escape differentiation and continue mitosis to form colonies in undifferentiating culture, cells could retain a fundamental feature of stem cell "i.e. the self renewal".

Taken together, although 3D alginate scaffold for hBM-MSCs could boost some of their functional aspects without combating their stemness characters, it did not support satisfactory cellular viability. Despite trying to probe the impact of encapsulation on these cells in various ways, the present data still have certain limitations; the issue of low cell survival per se needs further work to verify if the cause was merely the absence of adhesion moieties, or other factors as cell density and/or microcapsule size. The modulation of these factors could highly impact the behavior of immobilized cells (Santos et al., 2012). To date, it is not totally understood why MSCs endocytose alginate filament. Thus, such phenomenon should be studied comprehensively to realize its triggers and molecular basis and to investigate the possible influence of endocytosis on various cellular activities. Despite our provisional assessment of stemness criteria of cells before and after encapsulation, the question rises here is whether such retained stemness was quantitatively affected. This concern needs comprehensive quantitative assays in order to be answered. Additionally, sophisticated work is still to be done to explain the molecular bases behind altered behavior of hBM-MSCs upon encapsulation.

Conclusions

To sum up, hBM-MSCs show promising properties that entitle them to be a great choice for cell microencapsulation and cell-based therapy. The APA microencapsulation system has to overcome several challenges before being considered as a platform for long-term production of therapeutic factors. Though the enclosed cells seemed to be away from their natural microenvironment, their metabolic activity and productivity were enhanced. Additionally, stemness of the de-encapsulated cells was not lost. The ultrastructure of encapsulated cells was found to contribute to the better understanding of the behavioral and morphological changes of immobilized cells, albeit raising plenty of questions in need for answers regarding the molecular mechanisms underneath. Microencapsulation of hBM-MSCs in alginate-based bioscaffolds, as a relatively handy technique, might open new perspectives in treatment of various disorders.

Declaration of Interest

The authors report no conflict of interest. The authors alone are responsible for the content and writing of the article

Acknowledgements

N Attia thanks the Partnership and Ownership initiative (ParOwn) for receiving a mobility grant.

References

Abbah S, Lu W, Chan D, Cheung K, Liu W, Zhao F, Li Z, Leong J, Luk K. Osteogenic behavior of alginate encapsulated bone marrow stromal cells: An in vitro study. J Mater Sci Mater Med, 2008;19**:** 2113-9.

Abumaree M, Al Jumah M, Pace RA, Kalionis B. Immunosuppressive properties of mesenchymal stem cells. Stem Cell Rev, 2012;8**:** 375-92.

Baksh D, Song L, Tuan R. Adult mesenchymal stem cells: Characterization, differentiation, and application in cell and gene therapy. J Cell Mol Med, 2004;8**:** 301-16.

Baraniak PR, Mcdevitt TC. Scaffold-free culture of mesenchymal stem cell spheroids in suspension preserves multilineage potential. Cell Tissue Res, 2012;347**:** 701-11.

Beyth S, Borovsky Z, Mevorach D, Liebergall M, Gazit Z, Aslan H, Galun E, Rachmilewitz J. Human mesenchymal stem cells alter antigen-presenting cell maturation and induce T-cell unresponsiveness. Blood, 2005;105**:** 2214-9.

Bidarra SLJ, Barrias CC, Barbosa MRA, Soares R, Granja PL. Immobilization of human mesenchymal stem cells within RGD-grafted alginate microspheres and assessment of their angiogenic potential. Biomacromolecules, 2010;11**:** 1956-64.

Boomsma RA, Geenen DL. Mesenchymal stem cells secrete multiple cytokines that promote angiogenesis and have contrasting effects on chemotaxis and apoptosis. PLoS One, 2012;7**:** e35685.

Burchfield JS, Dimmeler S. Role of paracrine factors in stem and progenitor cell mediated cardiac repair and tissue fibrosis. Fibrogenesis Tissue Repair, 2008;1**:** 4.

Casanova J. Stemness as a cell default state. EMBO reports, 2012; 13: 396-7.

Chan BP, Hui TY, Yeung CW, Li J, Mo I, Chan GCF. Self-assembled collagen–human mesenchymal stem cell microspheres for regenerative medicine. Biomaterials, 2007; 28: 4652-66.

Correa PL, Mesquita CT, Felix RM, Azevedo JC, Barbirato GB, Falcão CH, Gonzalez C, Mendonça ML, Manfrim A, De Freitas G. Assessment of intra-arterial injected autologous bone marrow mononuclear cell distribution by radioactive labeling in acute ischemic stroke. Clin Nucl Med, 2007;32**:** 839-41.

Dominici M, Le Blanc K, Mueller I, Slaper-Cortenbach I, Marini FC, Krause DS, Deans RJ, KeatingA, Prockop DJ, Horwitz EM. Minimal criteria for defining multipotent mesenchymal stromal cells. The International Society for Cellular Therapy position statement. Cytotherapy, 2006; 8(4): 315-7.

Duggal S, Frønsdal KB, Szöke K, Shahdadfar A, Melvik JE, Brinchmann JE. Phenotype and gene expression of human mesenchymal stem cells in alginate scaffolds. Tissue Eng Part A, 2008;15**:** 1763-73.

Garate A, Murua A, Orive G, Hernández RM, Pedraz JL. Stem cells in alginate bioscaffolds. Ther Deliv, 2012;3**:** 761-74.

Ghidoni I, Chlapanidas T, Bucco M, Crovato F, Marazzi M, Vigo D, Torre ML, Faustini M. Alginate cell encapsulation: New advances in reproduction and cartilage regenerative medicine. Cytotechnology, 2008;58**:** 49-56.

Giordano A, Galderisi U, Marino IR. From the laboratory bench to the patient's bedside: An update on clinical trials with mesenchymal stem cells. J Cell Physiol, 2007;211**:** 27-35.

Gorbunov N, Garrison B, Zhai M, Mcdaniel D, Ledney G, Elliott T, Kiang J. Autophagy-mediated defense response of mouse mesenchymal stromal cells (MSCs) to challenge with Escherichia coli. DTIC Document 2012.

Goren A, Dahan N, Goren E, Baruch L, Machluf M. Encapsulated human mesenchymal stem cells: A unique hypoimmunogenic platform for long-term cellular therapy. FASEB J, 2010;24**:** 22-31.

Grayson WL, Zhao F, Izadpanah R, Bunnell B, Ma T. Effects of hypoxia on human mesenchymal stem cell expansion and plasticity in 3D constructs. J Cell Physiol, 2006; 207: 331–9.

Griffin MD, Ritter T, Mahon BP. Immunological aspects of allogeneic mesenchymal stem cell therapies. Hum Gene Ther, 2010;21**:** 1641-55.

Grossmann J. Molecular mechanisms of "detachment-induced apoptosis—anoikis". Apoptosis, 2002;7**:** 247-60.

Han S, Zhao Y, Xiao Z, Han J, Chen B, Chen L, Dai J. The three-dimensional collagen scaffold improves the stemness of rat bone marrow mesenchymal stem cells. J Genet Genomics, 2012.

Horie N, Pereira MP, Niizuma K, Sun G, Keren-Gill H, Encarnacion A, Shamloo M, Hamilton SA, Jiang K, Huhn S. Transplanted stem cell-secreted vascular endothelial growth factor effects poststroke recovery, inflammation, and vascular repair. Stem cells, 2011;29**:** 274-85.

Hu WS and Zeng AP. 2012. Genomics and systems biology of mammalian cell culture. Heidelberg, Germany: Springer.

Hunt NC, Smith AM, Gbureck U, Shelton RM, Grover LM. Encapsulation of fibroblasts causes accelerated alginate hydrogel degradation. Acta Biomaterialia, 2010; 6(9): 3649-56.

Jones E, Mcgonagle D. Human bone marrow mesenchymal stem cells in vivo. Rheumatology (Oxford), 2008;47**:** 126-31.

Karaöz E, Okçu A, Gacar G, Sağlam Ö, Yürüker S, Kenar H. A comprehensive characterization study of human bone marrow MSCs with an emphasis on molecular and ultrastructural properties. J Cell Physiol, 2011;226**:** 1367-82.

Kumar N, Gammell P, Clynes M. Proliferation control strategies to improve productivity and survival during CHO based production culture. Cytotechnology, 2007; 53: 33-46.

Lawson M, Barralet J, Wang L, Shelton R, Triffitt JT. Adhesion and growth of bone marrow stromal cells on modified alginate hydrogels. Tissue Eng, 2004;10**:** 1480-91.

Lee CS, Watkins EA, Burnsed OA, Schwartz Z, Boyan B. Tailoring adipose stem cell trophic factor production with differentiation medium components to regenerate chondral defects. Tissue Eng Part A, 2013; 19: 1451-64.

Lim F ,Sun AM. Microencapsulated islets as bioartificial endocrine pancreas. Science, 1980;210**:** 908-10.

Ma HL, Hung SC, Lin SY, Chen YL, Lo WH. Chondrogenesis of human mesenchymal stem cells encapsulated in alginate beads. J Biomed Mater Res A, 2003; 64: 273-81.

Markusen JF, Mason C, Hull DA, Town MA, Tabor AB, Clements M, Boshoff CH, Dunnill P. Behavior of adult human mesenchymal stem cells entrapped in alginate-GRGDY beads. Tissue Eng, 2006;12**:** 821-30.

Menasché P. Stem cells for clinical use in cardiovascular medicine. Thromb Haemost, 2005;94**:** 697-701.

Montironi R, Scarpelli M, Braccischi A, Galluzzi CM, Diamanti L, Alberti R. Quantitative analysis of nucleolar margination in diagnostic cytopathology. Virchows Arch A, 1991;419**:** 505-12.

Nauta AJ, Fibbe WE. Immunomodulatory properties of mesenchymal stromal cells. Blood, 2007;110**:** 3499-506.

Nagaya N, Takafumi F, Takashi I, Hajime O, Takefumi I, Masaaki U, Masakazu Y, Hidezo M, Kenji K, Soichiro K. Intravenous administration of mesenchymal stem cells improves cardiac function in rats with acute myocardial infarction through angiogenesis and myogenesis. Am J Physiol Heart Circ Physiol, 2004;287: H2670-6.

Neuhuber B, Swanger SA, Howard L, Mackay A, Fischer I. Effects of plating density and culture time on bone marrow stromal cell characteristics. Exp Hematol, 2008;36**:** 1176-85.

Ngoc PK, Van Phuc P, Nhung TH, Thuy DT, Nguyet NTM. Improving the efficacy of type 1 diabetes therapy by transplantation of immunoisolated insulin-producing cells. Hum Cell, 2011;24**:** 86-95.

Nunamaker, EA, Erin KP, Daryl RK. In vivo stability and biocompatibility of implanted calcium alginate disks. J Biomed Mater Res A, 2007; 83.4: 1128-37.

Orive G, Carcaboso A, Hernandez R, Gascon A, Pedraz J. Biocompatibility evaluation of different alginates and alginate-based microcapsules. Biomacromolecules, 2005;6**:** 927-31.

Orive G, Hernández RM, Gascón AR, Pedraz JL. 2006. Encapsulation of cells in alginate gels. In: Guisan JM, ed. Immobilization of enzymes and cells. New Jersey: Humana Press 345-55.

Pasquinelli G, Tazzari P, Ricci F, Vaselli C, Buzzi M, Conte R, Orrico C, Foroni L, Stella A, Alviano F. Ultrastructural characteristics of human mesenchymal stromal (stem) cells derived from bone marrow and term placenta. Ultrastruct Pathol, 2007;31**:** 23-31.

Phinney DG, Prockop DJ. Concise review: Mesenchymal stem/multipotent stromal cells: The state of transdifferentiation and modes of tissue repair—current views. Stem cells, 2007;25**:** 2896-902.

Pittenger MF, Martin BJ. Mesenchymal stem cells and their potential as cardiac therapeutics. Circ Res, 2004;95**:** 9-20.

Ponce S, Orive G, Hernández R, Gascón AR, Pedraz JL, De Haan BJ, Faas MM, Mathieu H, De Vos P. Chemistry and the biological response against immunoisolating alginate–polycation capsules of different composition. Biomaterials, 2006;27**:** 4831-9.

Ranganath SH, Levy O, Inamdar MS, Karp JM. Harnessing the mesenchymal stem cell secretome for the treatment of cardiovascular disease. Cell Stem Cell, 2012;10**:** 244-58.

Rowlands AS, George PA, Cooper-White JJ. Directing osteogenic and myogenic differentiation of mscs: Interplay of stiffness and adhesive ligand presentation. Am J Physiol Cell Physiol, 2008;295**:** C1037-C44.

Sanchez-Ramos JR. Neural cells derived from adult bone marrow and umbilical cord blood. J Neurosci Res, 2002;69**:** 880-93.

Santos E, Orive G, Calvo A, Catena R, Fernández-Robredo P, Layana AG, Hernández RM, Pedraz JL. Optimization of 100 μm alginate-poly-L-lysine-alginate capsules for intravitreous administration. J Control Release. 2012; 158(3):443-50.

Sasaki K, Matsumura G, Ito T. A quantitative morphology of nucleoli of erythroblasts in the mouse spleen: An electron microscopic study. Arch Histol Jpn, 1983;46**:** 43-9.

Sayyar B, Dodd M, Wen J, Ma S, Marquez-Curtis L, Janowska-Wieczorek A, Hortelano G. Encapsulation of factor IX–engineered mesenchymal stem cells in

fibrinogen–alginate microcapsules enhances their viability and transgene secretion. J Tissue Eng, 2012;3**.**

Shin L, Peterson DA. Human mesenchymal stem cell grafts enhance normal and impaired wound healing by recruiting existing endogenous tissue stem/progenitor cells. Stem Cells Transl Med, 2013; 2: 33-42.

Spicer S, Parmley R, Boyd L, Schulte B. Giant mitochondria distinct from enlarged mitochondria in secretory and ciliated cells of gerbil trachea and bronchioles. Am J Anat, 1990;188**:** 269-81.

Tandler B, Nagato T, Phillips CJ. Megamitochondria in the serous acinar cells of the submandibular gland of the neotropical fruit bat, artibeus obscurus. Anat Rec, 1997;248**:** 13-7.

Tang J, Xie Q, Pan G, Wang J, Wang M. Mesenchymal stem cells participate in angiogenesis and improve heart function in rat model of myocardial ischemia with reperfusion. Eur J Cardiothorac Surg 2006;30**:** 353-61.

Tso GHW, Law HKW, Tu W, Chan GCF, Lau YL. Phagocytosis of apoptotic cells modulates mesenchymal stem cells osteogenic differentiation to enhance IL-17 and RANKL expression on CD4+ T cells. Stem cells, 2010;28**:** 939-54.

Wachtler F, Hopman A, Wiegant J, Schwarzacher H. On the position of nucleolus organizer regions (NORs) in interphase nuclei: Studies with a new, non-autoradiographic in situ hybridization method. Exp Cell Biol, 1986;167**:** 227-40.

Yu J, Du KT, Fang Q, Gu Y, Mihardja SS, Sievers RE, Wu JC, Lee RJ. The use of human mesenchymal stem cells encapsulated in RGD modified alginate microspheres in the repair of myocardial infarction in the rat. Biomaterials, 2010;31**:** 7012-20.

Figure legends

FIGURE 1. Morphological characteristics of hBM-MSCs. Cells appeared as a heterogeneous population of cells. They exhibited large, flattened, or fibroblast-like shapes. (**A**): day 1, (**B**): day 7 culture. (**C**) After 14 days of hBM-MSC culture, adjacent interconnected colonies stained with crystal violet. (**D**) Adipogenic differentiation wells depicted intracellular lipid droplets stained with ORO. (**E**) Osteogenic differentiation was characterized by the deposition of amorphous material positively stained with ARS. (**F, G**) Control cultures did not show any positive staining. Mag. (**A, B, D, E, F, G**) x100, (**C**) x40.

FIGURE 2. (**A**) Bright field (Upper panel) and fluorescence (Middle panel) micrographies of encapsulated hBM-MSCs stained with the LIVE/DEAD kit. Microcapsules depicted uniform rounded contour. Green dots represented cytoplasm of living cells, while red dots represented the nuclei of dead cells. Majority of cells appeared evenly dispersed and viable throughout the microcapsule. Scale bar: 200 µm. Lower panel show flow cytometry-based viability for hBM-MSCs exposed to alginate lyase de-encapsulation procedure, performed on days 1, 14, and 42 post-immobilization. The FL1/FL3 dot-plots of calcein/ EthD-1 labeled cells. Upper left quadrants represented live cells. Lower right quadrants represented dead cells, while upper right quadrants represented cells with impaired plasma membranes. The dimensions of all the quadrants were held constant when calculating cell viability in all experiments. (**B**) Line graph representing number of living cells/capsule.

FIGURE 3. (**A, B**) Line graphs reported the metabolic activity of viable cells by CCK-8 assay on days 1, 7, 14, 21, 28, 35 and 42 of culture. (**A**) Monolayer cells (n=3), (**B**) Encapsulated cells (n=7). (**C**) Bar graph showing BrdU uptake of encapsulated hBM-MSCs, demonstrated no significant increase in BrdU incorporation, neither on day 10 nor on day 30 post-encapsulation ($p>0.05$) (n=5). (**D**) Bar graph showing VEGF secretion of hBM-MSCs. As monolayer cultures, day1 and day 28 post-encapsulation (n=3). Their secretion significantly increased after encapsulation ($P=0.05$), with no significant change later ($P> 0.05$). Vertical error bars represented the standard deviation of the reported mean values. (∗ = statistical significance) (NS= no significance).

FIGURE 4. Filamentous actin network of encapsulated hBM-MSCs stained with Alexa Fluor 488-Phalloidin. Short cytoplasmic processes projecting out of cell surface after 2 weeks of encapsulation that appeared longer after 4 weeks (arrow heads). (**A, C**) showed optical slices through 2 & 4 weeks immobilized cells, respectively. (**B, D**) showed 3D reconstruction of the same cells. (Scale bars: 10 μm).

FIGURE 5. Transmission electron micrographs. (**A,B**) monolayer hBM-MSC depicting: (**A**) an eccentric, irregularly shaped and large euchromatic nucleus (N) with prominent nucleolus (nu). The cell surface showed many thin pseudopodia (asterisk); (**B**) higher magnification of the marked area in A. The cytoplasm was particularly rich in rough endoplasmic reticulum (rER) with dilated cisternae containing moderately electron dense material. Clear vacuoles (V) located mainly at the periphery of the cell cytoplasm. (**C, D**) 2 weeks immobilized hBM-MSCs. The cytoplasm depicted several vacuoles (V) of variable sizes with alginate filaments internalized in some of them

similar to the extra cellular ones (thin arrows). Abundant rER profiles and mitochondria (arrow heads) were seen. (**A**) Encapsulated cell near the surface of the microcapsule (grey arrow). (**E,F**) hBM-MSCs after 4 weeks of encapsulation depicting euchromatic nuclei (N), marginated nucleolus (nu), and several vacuoles (V) of variable sizes-some depicted internalized alginate filaments (thin arrows). Abundant rER profiles and giant mitochondria (M) were seen. Lysosomes (white arrow) were observed in the cytoplasm. Uranyl acetate and lead citrate stain, (scale bars **A**: 5 μm, **B**-**F**: 2 μm).

FIGURE 6. (**A**) Differentiation of microcapsule de-encapsulated hBM-MSCs into fat (left panel, ORO staining) and bone (middle panel, ARS staining). Right panel shows representative negatively stained undifferentiated de-encapsulated hBM-MSCs. Assay was performed after 2, 4 and 6 weeks of encapsulation. (Mag. x100). (**B**) Crystal violet staining of adjacent interconnected colonies of hBM-MSCs; a: before encapsulation, b: de-encapsulated after 6 weeks of encapsulation. (Mag. x40).

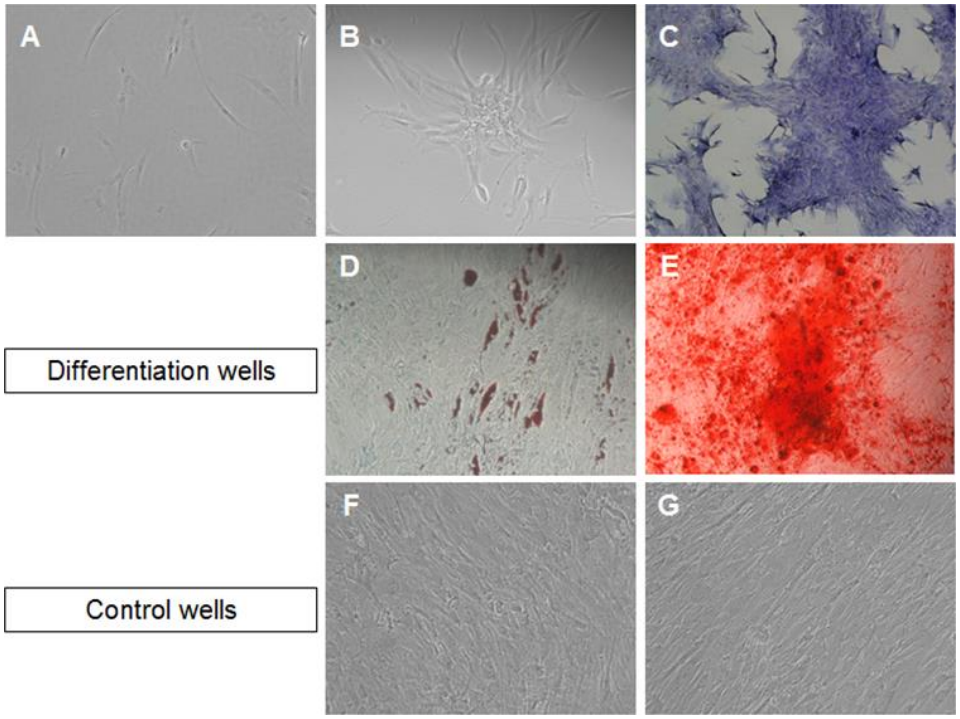

Figure 1.

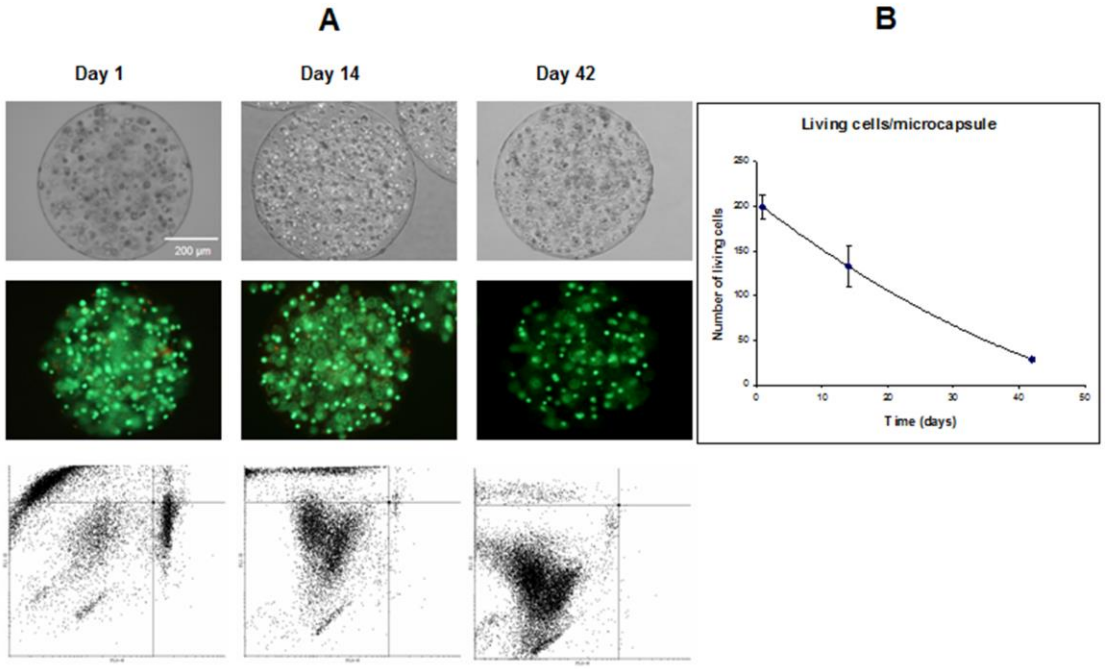

Figure 2.

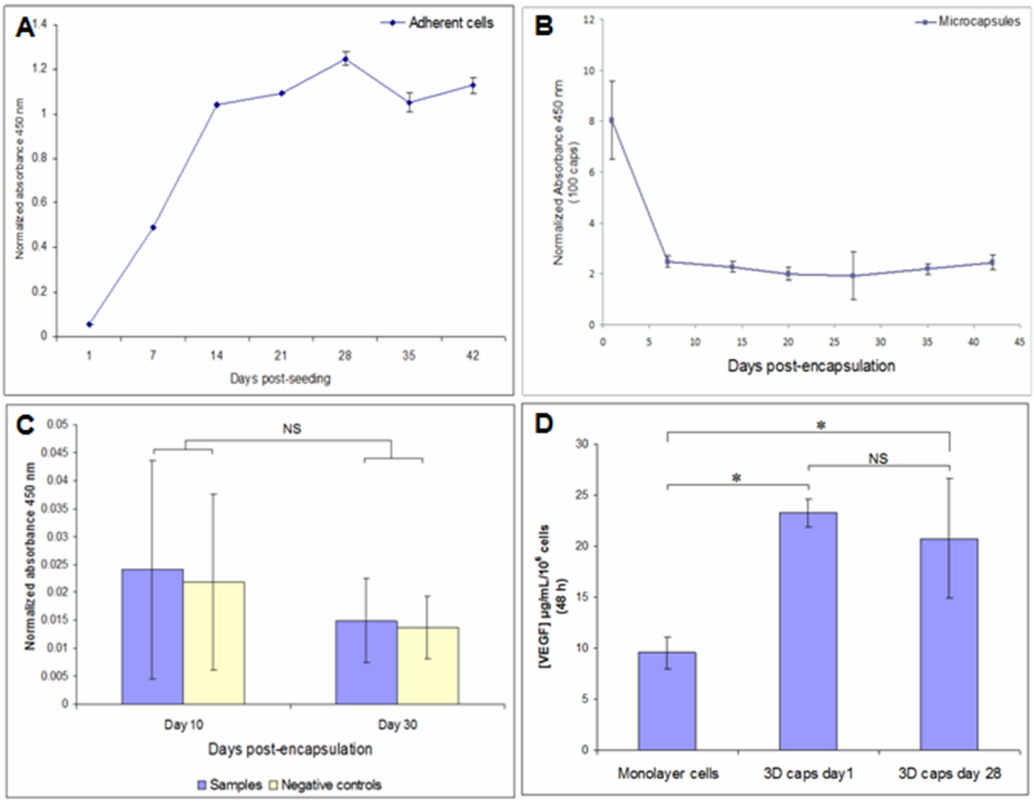

Figure 3.

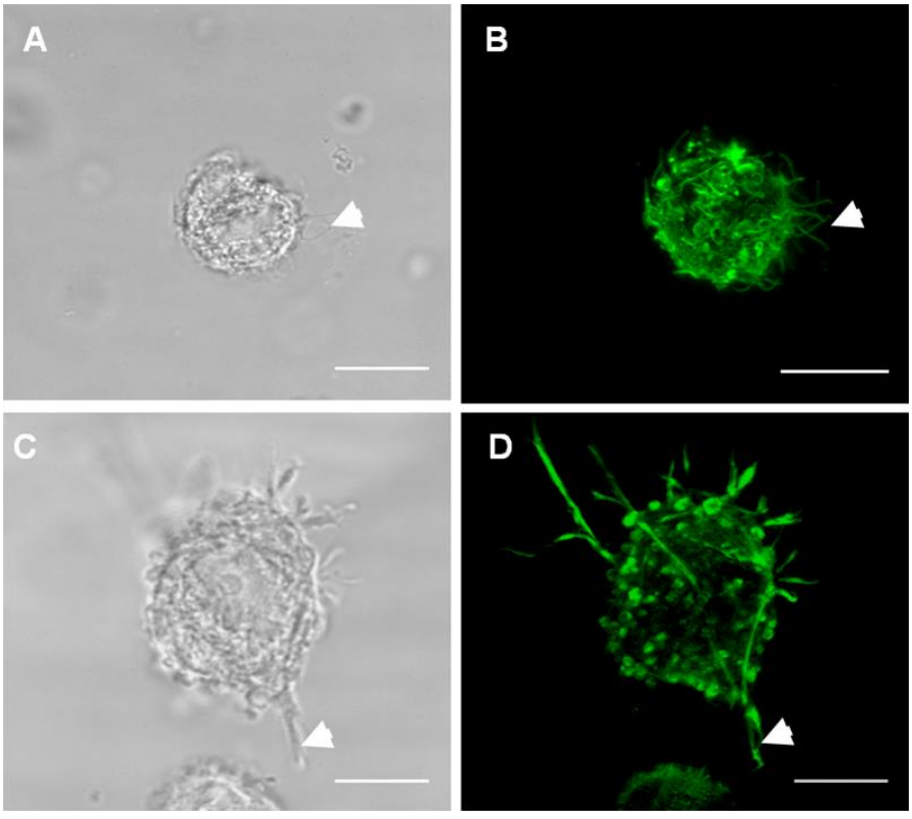

Figure 4.

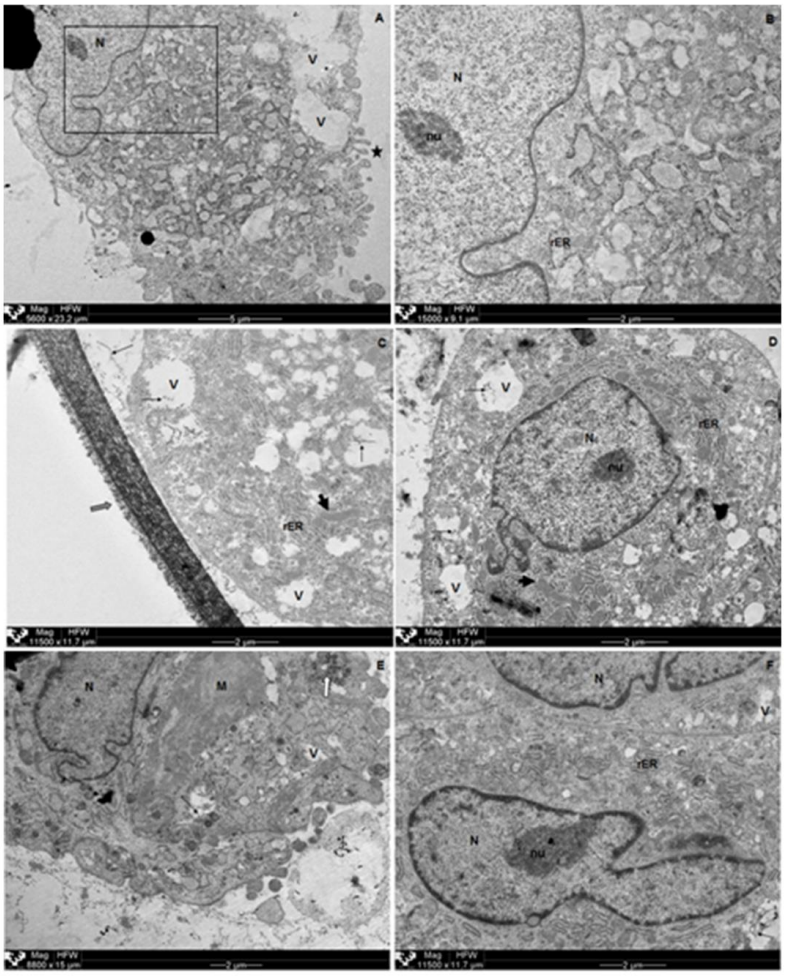

Figure 5.

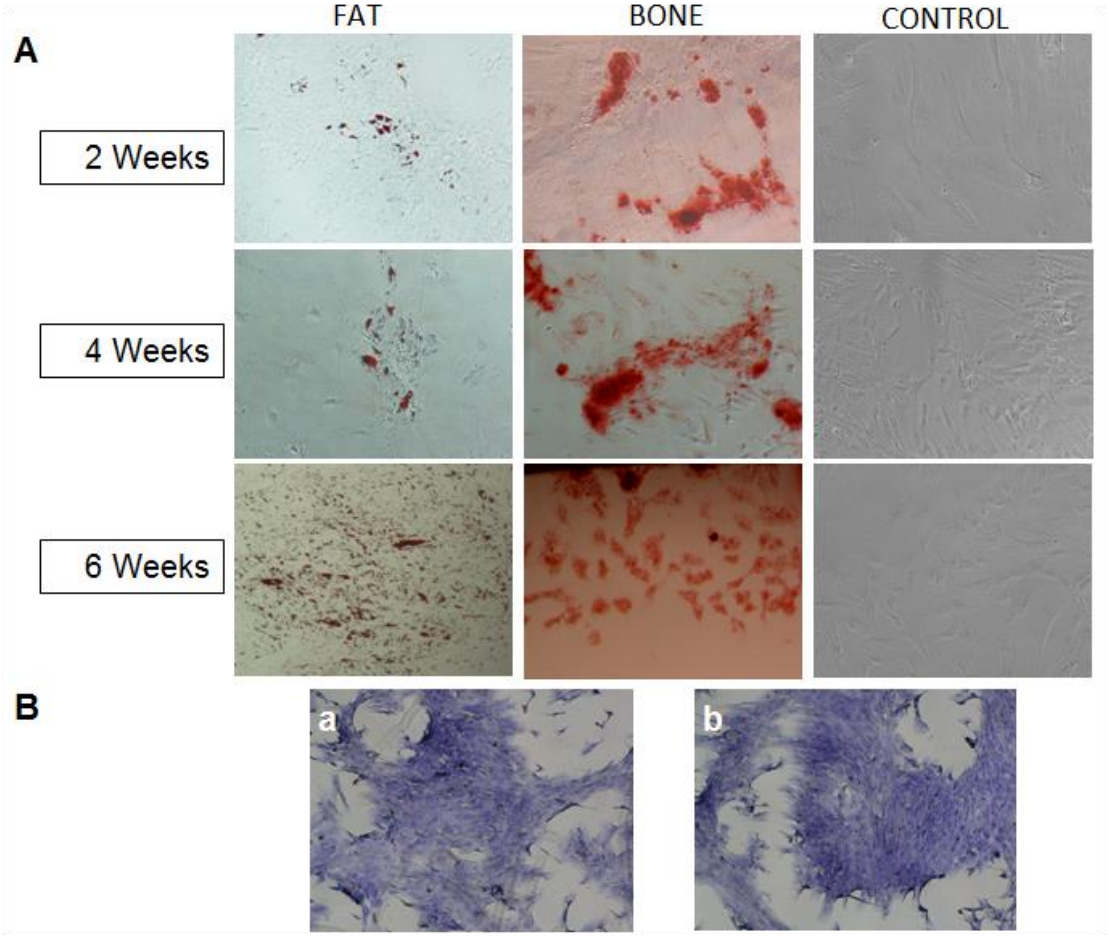

Figure 6.